Hindawi
Shock and Vibration
Volume 2019, Article ID 9056810, 12 pages
https://doi.org/10.1155/2019/9056810

Research Article

Dynamic Response of a Single-Layer Reticulated Dome during Aircraft Impact Based on S-J Modeling Method

Li Lin,[1,2] **Bo Huang**,[1] **Yunhui Sun**,[1] **Yu Zhu**,[1] **and Duozhi Wang**[3]

[1]*College of Civil Engineering and Architecture, Harbin University of Science and Technology, Harbin 150080, China*
[2]*School of Civil Engineering, Harbin Institute of Technology, Harbin 150080, Heilongjiang, China*
[3]*Institute of Engineering Mechanics, China Earthquake Administration, Harbin 150080, China*

Correspondence should be addressed to Li Lin; 13766899951@163.com

Received 26 March 2019; Revised 11 August 2019; Accepted 20 August 2019; Published 9 September 2019

Academic Editor: Yuri S. Karinski

In previous numerical models developed for the impact dynamic responses of reticulated domes, mostly BEAM 161 elements and piecewise linear plastic material model have been employed and spherical joints have been simplified as intersection points of beams, which is called the B-P method. The B-P method can be employed in studying the dynamic responses of reticulated shells under low- to moderate-speed impacts with no obvious temperature effect. However, the analysis of the dynamic responses of reticulated shells under moderate- and high-speed impacts of missiles and other aircraft using this method had errors because it could not take into account the temperature effect. To accurately describe the mechanical responses of reticulated shells under aircraft impacts, the Johnson–Cook material model considering temperature effect with corresponding SHELL 163 element was selected for determining the members of the numerical model and the shell element was used to establish the spherical joints of reticulated shells; the whole process was called the S-J modeling method. This modeling method was capable of considering the effects of high strain rates, high temperatures, large strains, stress state change, and loading history. S-J and B-P methods were used to model the reticulated shell structures. Comparing the numerical analysis results of the drop hammer impact of the two developed methods with experimental results verified the accuracy of the S-J modeling method. In addition, based on the results obtained from the S-J modeling method and LS-DYNA finite element analysis software, a numerical model was established for small aircraft impact reticulated shells and the failure modes and dynamic responses of reticulated shell structures under aircraft impacts were studied. In terms of energy analysis, it was found that the effects of roof plates, spherical joints, and temperature softening could not be ignored in such studies.

1. Introduction

Reticulated domes are one of the main forms of large structures with high political, economic, and cultural significance since they are usually used in large public buildings [1, 2]. Zhai studied the response types and the functions of protective measures of Kiewitt8 single-layer reticulated shells subjected to internal blast loading [3, 4]. Nie investigated the seismic behavior of reticulated domes through shaking table tests and invented an innovative isolated support for 3D isolation [5]. Xu proposed the DEM algorithm for progressive collapse simulation of single-layer reticulated domes under multisupport excitation [6]. Le et al. showed that the material properties of reticulated dome structures and their components had significant effects on their impact resistance [7]. Li et al. conducted scaled model tests of K8 single-layer reticulated domes under drop hammer impacts and measured their dynamic responses and destructive processes [8, 9]. Wang conducted systematic studies on the impact resistance of Kiewitt8 single-layer reticulated domes and revealed their failure mechanisms and energy transmissions in structures [10, 11]. Wang conducted impact tests and numerical simulations on single-layer spherical reticulated domes and investigated their dynamic responses and failure modes [12, 13].

Previous research works have rarely been focused on the behavior of reticulated domes during aircraft impacts. Lin [14, 15] developed a numerical aircraft impact model and

investigated multiple positions on the reticulated domes and possible failure modes during aircraft collisions for different flight modes. Yin studied the failure modes of K8 reticulated domes during aircraft impact using a numerical model based on BEAM 161 and a piecewise linear plastic material model using spherical joints with no roof sheathing [16].

Research on the impact resistance of reticulated domes has mainly been concentrated on failure modes and mechanisms and limited to low-speed impacts. Also, previous numerical analyses have mainly adopted the B-P method for modeling, BEAM 161 element as members, and piecewise linear plastic material model for material properties and have simplified spherical joints as intersection points of beams. This modeling method is feasible under low- and moderate-speed collisions with minor temperature effects. However, for high-speed or hypervelocity collisions, temperature effects cannot be ignored and the aforementioned model creates significant errors.

To precisely describe the mechanical responses of reticulated shell structures under aircraft impacts, the Johnson–Cook material model considering temperature effect with corresponding SHELL 163 element was selected to determine the members of the numerical model and the shell element was used to establish the spherical joints of reticulated shells; the whole process was called the S-J modeling method. This method could take into account the effects of high strain rates, high temperatures, large strains, stress state change, and loading history, and drop-weight tests were used to verify the accuracy of the proposed numerical model. A numerical model was developed for a K8 single-layer spherical reticulated dome and a Bombardier Challenger 850 small aircraft based on S-J modeling. The behavior of reticulated dome during aircraft collision was simulated to determine its failure mode and analyze its dynamic response without considering the explosion of aircraft.

2. S-J Modeling Method

Previous numerical models developed for the dynamic responses of reticulated domes under impact loading have generally employed BEAM 161 element members and the piecewise linear plastic material model, and spherical joints have been simplified as intersection points of beams ; the whole process is called the B-P method. This method is more applicable to low- and moderate-speed impacts and has significant errors when used for high-speed or hypervelocity collisions since it cannot take into account the temperature effect. Therefore, the S-J method was proposed with the Johnson–Cook model for material properties, and SHELL 163 element as members of the numerical model of reticulated shell structures and shell element was used to establish spherical joints of reticulated shells.

2.1. Material Model. Previous piecewise linear plastic material models have generally adopted the Cowper–Symonds model which considers the strain rate as

$$\sigma_y = \left[1 + \left(\frac{\dot{\varepsilon}}{C}\right)^{1/p}\right]\left(\sigma_0 + f_h\left(\varepsilon_{\text{eff}}^p\right)\right), \quad (1)$$

where σ_0 is the yield stress under a common strain rate, ε is the effective strain rate, and C and p are the strain rate parameters where for steel $C = 40$ and $p = 5$. $f_h(\varepsilon_{\text{eff}}^p)$ is a hardening function based on effective plastic strain.

The Johnson–Cook constitutive model considers the effects of strain, strain rate strengthening, and temperature softening and can be written as

$$\sigma = \left(A + B\varepsilon_{\text{eq}}^n\right)\left(1 + C\ln\dot{\varepsilon}^*\right)\left(1 - T^{*\text{m}}\right), \quad (2)$$

where A, B, n, C, and m are the material constants, ε_{eq} is the equivalent plastic strain, $\dot{\varepsilon}^*$ is a dimensionless equivalent plastic strain, $\dot{\varepsilon}^* = \dot{\varepsilon}/\dot{\varepsilon}_0$, $\dot{\varepsilon}_0$ is a reference strain rate, $T^* = (T - T_r)/(T_m - T_r)$ is a dimensionless temperature parameter in which T is the material temperature, T_r is a reference temperature (usually set to room temperature), and T_m is the melting point of the considered material [17].

The Johnson–Cook fracture criterion was defined as

$$\varepsilon_f = \left[D_1 + D_2\exp\left(D_3\sigma^*\right)\right]\left(1 + D_4\ln\dot{\varepsilon}^*\right)\left(1 + D_5T^*\right), \quad (3)$$

where D_1–D_5 are the material parameter and σ^* is the stress triaxiality. Based on a series of material quality tests, the relationships between strength and equivalent plastic strain, strain rate, temperature, fracture strain, and stress triaxiality were obtained, and parameter calibration is shown in Table 1.

In addition to the two abovementioned modeling methods, a piecewise elastic-plastic model has been developed which considers the effect of strain rate and is widely used in low- and moderate-speed collisions. In the Johnson–Cook material model, the effects of stress triaxiality, temperature, and strain rate on failure strain can be considered in tandem. A Taylor impact test was conducted to select the most suitable material model for high-velocity collisions.

A comparison between the results obtained from numerical simulation and Taylor test with those obtained from the Johnson–Cook material model is shown in Figure 1. Simulation results were similar to the test results which verified the viability of the Johnson–Cook model. Comparison of simulation results with those of the Taylor test with the piecewise linear constitutive model is shown in Figure 2. As can be seen in the figure, upsetting, cracking, and petaling failures were evident when stress triaxiality and strain rate were reasonably considered, but the velocity interval corresponding to a fracture model could not be obtained simultaneously with the same set of parameters. Take the same section of data acquired from the test, then adjust the parameters of stress triaxiality and strain rate; if cracking failure at low speed can be predicted reasonably, the projectile body will undergo fragmenting failure at high speeds, and if petaling failure can be reasonably predicted at high speeds, cracking failure cannot take place at low speeds, as shown in Figure 2.

The effect of temperature on the constitutive model and failure cannot be considered in the piecewise linear model,

Table 1: Material constants of Q235B steel.

E (GPa)	ν	ρ (kg/m^3)	Cp (J/kgK)	T_r (K)	T_m (K)	$\dot{\varepsilon}$ (s^{-1})	χ	A (MPa)	B (MPa)
200	0.3	7800	469	293	1795	$8.33e-4$	0.9	244.8	899.7
n	m	F	C	D_1	D_2	D_3	D_4	D_5	D_6
0.940	0.151	1.989	0.0391	−43.408	44.608	−0.016	0.0145	−0.046	7.776

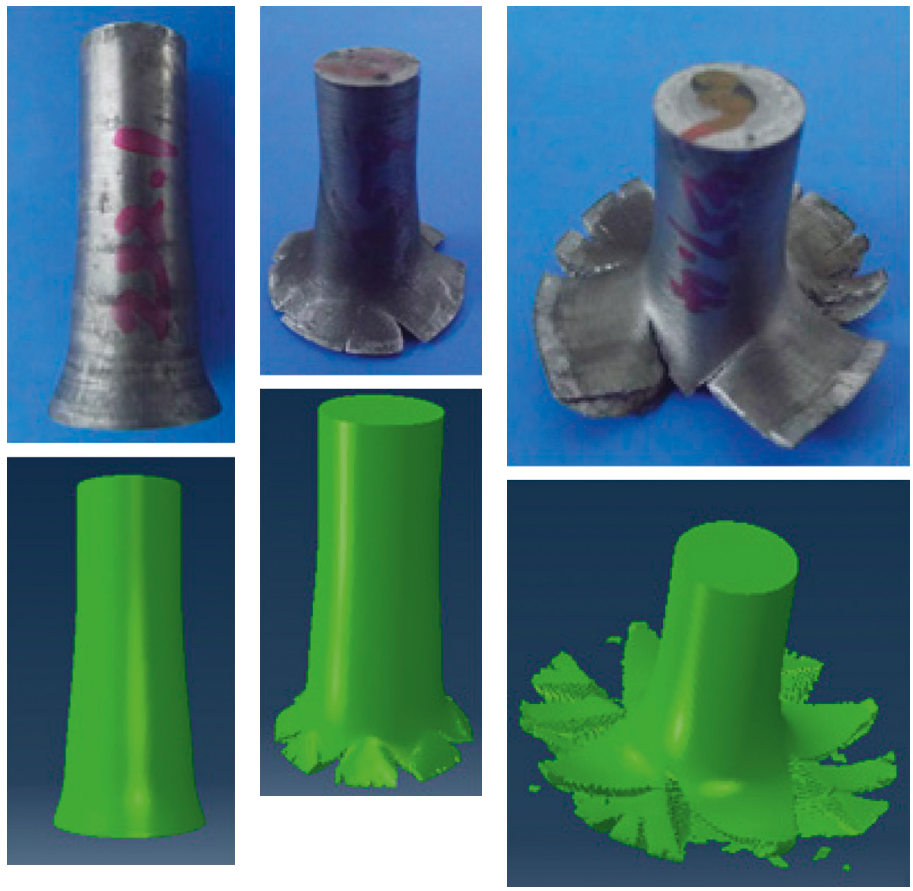

(a) (b) (c)

Figure 1: Comparison of numerical simulation and Taylor test results. (a) v = 232.1 m/s. (b) v = 232.1 m/s. (c) v = 437.4 m/s.

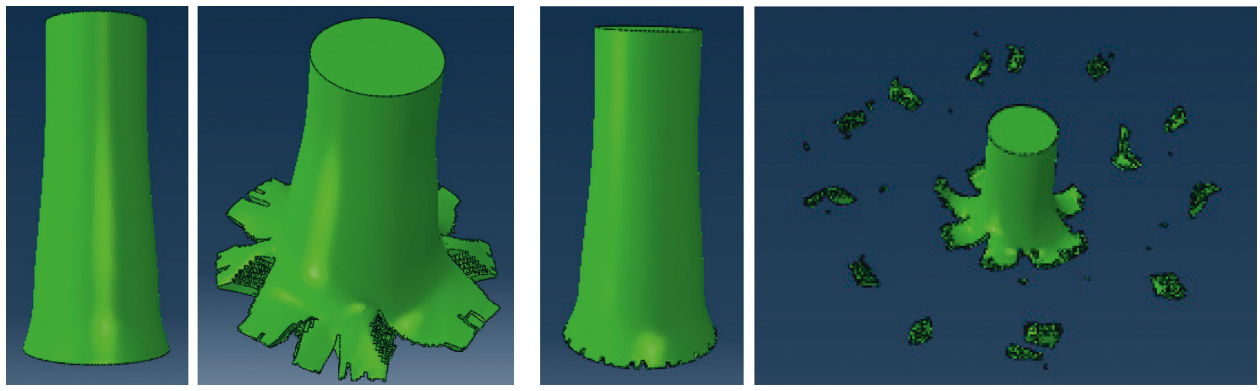

(a) (b)

Figure 2: Predicted results using the piecewise linear model. (a) The first group of parameters. (b) The second group of parameters.

which may be the reason for the inconsistency of the predicted velocity interval and test results. If the piecewise linear model could be sufficiently discretized and the effects of strain rate and temperature could be taken into account in the failure mode, the proposed model could be considered as a generalized form of the Johnson–Cook model, and this verifies the usefulness of the proposed model in describing deformation and fracture under high strain rates.

2.2. Contact Type and Element Type. In this work, a single-layer spherical reticulated dome was considered as the simulation object. The main bar material was assumed to be a thin-walled seamless circular steel tube; however, the common BEAM 161 element could not be selected when using the Johnson–Cook model. Therefore, SHELL 163 element was employed in the numerical model of the reticulated dome which could display nonlinear behavior during dynamic analysis.

Generally, large distortions occur during dynamic analysis, and the determination of contact type between parts is very difficult in the model. Therefore, the determination of contact type is an important task in collision simulations. In ANSYS/LS-DYNA software, three basic contact types can be defined: single-surface contact, node-surface contact, and surface-surface contact [18].

The single-surface contact is used for self-contacts in a single object or simple contacts between two objects. In the node-surface contact, the contact node penetrates the target surface and is usually used to describe contacts between two surfaces. The surface-surface contact happens when one object penetrates the surface of another object and is usually used to describe contacts between objects with arbitrary shapes and large contact areas.

Single-surface and surface-surface contacts could be selected in this paper. The AG contact (custom contact) has the characteristics of simple definition, convenient application, and accurate calculation results.

LS-DYNA software contains 3 contact algorithms: penalty function, node constraint, and distribution parameter methods. Node constraint method is applied to solid connection surfaces, and distribution parameter method is suitable for gas and fluid convective structures. Distribution parameter method is a common algorithm used to prevent penetration by adjusting the penalty function value and time step. It is suitable for simulations involving large deformations during collision. Thus, the distribution parameter method was selected in this study.

2.3. Connection between Bars and Spherical Joints. The geometric relationship between bars and spherical joints can be described with Boolean operations. The Boolean subtraction was used to discard redundant members in a node. Bar surface was subtracted from node surface, and thus the bar was divided into two parts by the spherical shell after the intersecting bar in the spherical node is deleted. It has to be noted that the column joint face should not be subtracted from bar surface because if so, a number of small circular surfaces would be segmented from node surface. This would create a hole in spherical surface which could make troubles in the following cell partition operations.

Then, the connections between bars and spherical joints could be decomposed using a Boolean operation. The AGLUE command was used to divide cells. This way, some elements might be malformed and could not be decomposed using the proposed method. A tolerance threshold had to be set after dividing cells, and the AGLUE command could be used to connect members and nodes. Cells could be partitioned using the AATT command, shown in Figure 3.

Hence, the S-J method with the Johnson–Cook material model and SHELL 163 element was proposed to build a numerical model for reticulated domes, and spherical joint connections were used at the end of bars. This method could consider the effects of high strain rates, high temperatures, large strains, stress state change, and loading history.

3. Verification of S-J Method by Drop-Weight Test

In order to verify the applicability of the S-J method, it was used to establish two numerical models for a single-layer spherical dome with 1800 mm span and the span to rise ratio of 9.23, as shown in Figure 4. The locations of strain gauges in machining and reticulated shell models are shown in Figure 5.

Elastic impacts after 8 and 10 mm drops and damage resulting from a 3.2 m drop were analyzed using the S-J method. The obtained results were compared with those of the drop-weight test reported by Lin of Harbin Institute of Technology (HIT) [14] and numerical results from the B-P method.

Table 2 shows the numerical deviation of the results obtained from the numerical model without roof sheathing from the test results under elastic impact. As shown in Table 2, simulation results obtained from the S-J modeling method were slightly larger than the test results with acceptable error ranges, and among them, stress H1 was very close to the test results. Compared with simulation results obtained from the B-P method, errors from dynamic response characteristics index of the S-J method were relatively small and numerical calculations were more stable. Hence, the validity of the model without roof sheathing built by the S-J method was confirmed.

Errors in numerical analyses and test results with roof sheathing under elastic impact are shown in Table 3. From Table 3, the first impact duration and stress value predicted by the S-J method were very close to the test results and the error of Stress H1 was even lower than 5%. Compared to the B-P method, errors had obviously been decreased. For the time interval between first and second impacts, the numerical simulation result of the S-J method under 8 and 10 mm impacts were 41.37% and 29.89% larger than the test results, respectively. This was because a certain damping exists in the actual reticulated domes with roof sheathing during tests, energy loss when the vertex node was impacted in the drop-weight test was larger than that in numerical simulation so that bounce height after impact in the test was lower than that in numerical simulation. More attention has

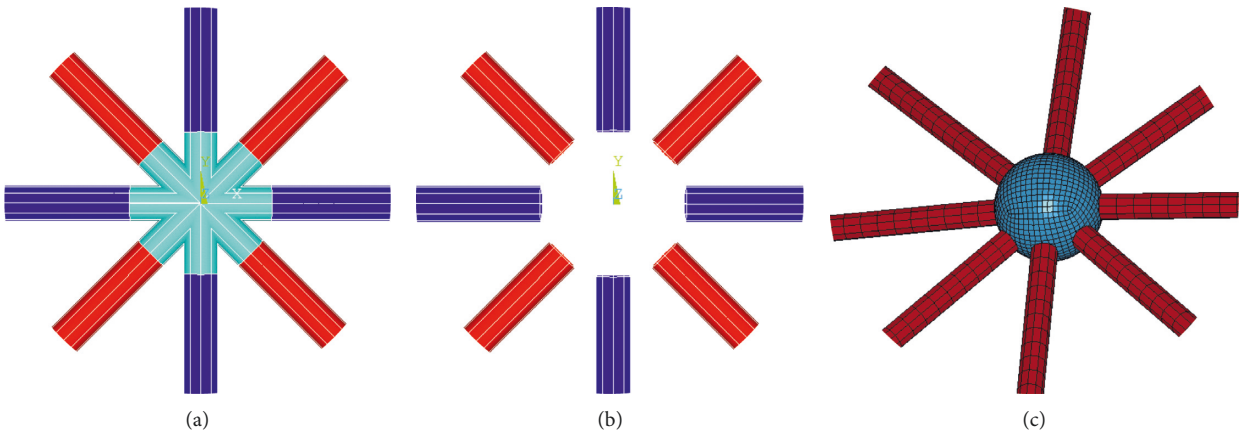

(a) (b) (c)

Figure 3: Process of connection between bars and spherical joints. (a) Boolean operation. (b) Deletion of redundant members. (c) Element mesh generation.

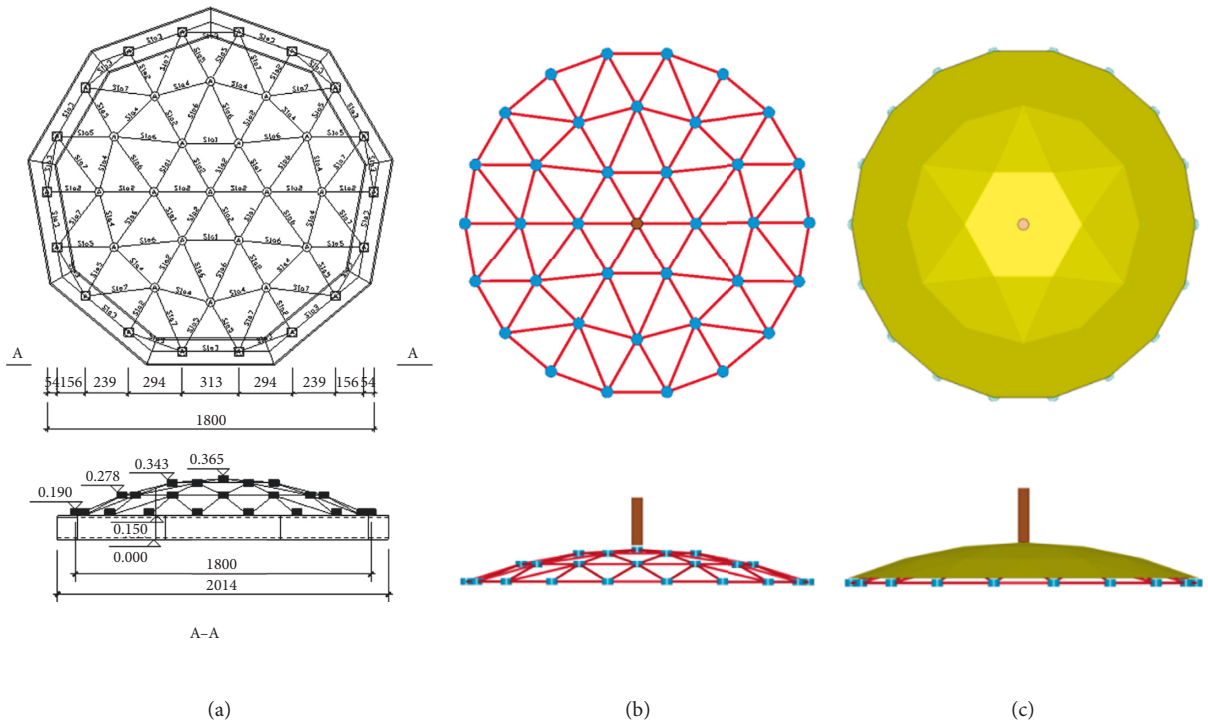

(a) (b) (c)

Figure 4: Scale model and numerical model. (a) Reticulated shell model of test. (b) Reticulated shell model without roof plate. (c) Reticulated shell model with roof plate.

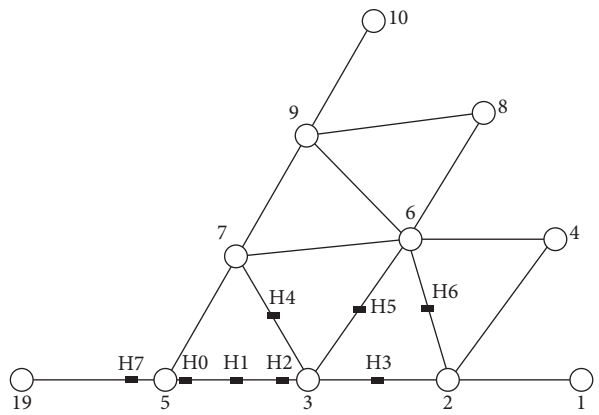

Figure 5: Gauge locations on the scale model of reticulated shells.

Table 2: Deviation between numerical and test results without roof sheathing.

Impact type (mm)	Comparison program	Test	B-P		S-J	
		Value	Value	Error (%)	Value	Error (%)
8	First impact duration (ms)	32.90	31.50	−4.25	42.20	28.27
	Stress H1 (MPa)	−81.90	−91.80	12.09	−78.70	−3.91
	Stress H4 (MPa)	38.10	47.10	23.62	32.20	−15.49
	Time interval (ms)	49.10	73.60	49.90	47.10	−4.1
10	First impact duration (ms)	33.80	36.00	6.51	41.20	21.89
	Stress H1 (MPa)	−96.50	−99.00	2.59	−96.20	−0.31
	Stress H4 (MPa)	44.50	37.50	−15.73	35.60	−20.00
	Time interval (ms)	61.70	88.80	43.92	68.60	11.18

Table 3: Deviations between the numerical and test results with roof sheathing.

Impact type (mm)	Comparison program	Test	B-P		S-J	
		Value	Value	Error (%)	Value	Error (%)
8	First impact duration (ms)	20.60	23.30	13.11	19.10	−7.28
	Stress H1 (MPa)	−68.40	−57.50	−15.94	−70.60	3.22
	Stress H4 (MPa)	42.60	48.00	12.68	36.60	−14.08
	Time interval (ms)	42.30	70.20	65.96	59.80	41.37
10	First impact duration (ms)	20.20	23.10	14.36	19.00	−5.94
	Stress H1 (MPa)	−76.80	−63.80	−16.93	−79.30	3.26
	Stress H4 (MPa)	47.50	56.00	17.89	40.50	−14.74
	Time interval (ms)	54.20	83.70	54.43	70.40	29.89

to be paid to response after the first impact to make the errors of time intervals below 50% acceptable. In addition, compared to the B-P method, errors at two conditions had obviously been decreased. Hence, the validity of the model with roof sheathing built by the S-J method was confirmed.

Under 3.2 m destructive impact, the results obtained for the failure mode of the simulated reticulated dome without roof sheathing were similar to the test results, where all structural members collapsed. However, the failure mode of simulated reticulated dome with roof sheathing gave similar results to the test results, where partial depression occurs, as shown in Figure 6. This demonstrated the accuracy of the proposed model.

The transformation of steel in the impact zone during aircraft collision usually involves large strains, high stain rates, and temperature softening. The Johnson–Cook material model can describe collisions under these conditions, and SHELL 163 elements can properly describe the members of reticulated dome structures, spherical joints, and roof sheathing. Hence, the S-J method was used to model reticulated domes in this work.

4. Failure Mode during Aircraft Collision

4.1. Aircraft Model. In order to better examine damage process in a reticulated dome, a Bombardier Challenger 850 was selected as a prototype because its size was suitable. External total length was 26.77 m, total width was 6.22 m, and wingspan was 21.21 m.

During aircraft modeling process, structural details such as windows and doors were simplified and their effects during aircraft impact and subsequent explosions after collision were ignored. The size of the aircraft numerical model basically agreed with that of the aircraft entity model. Aircraft structure is very complicated, and it is very difficult to design its geometry in ANSYS/LS-DYNA. Therefore, first outline drawing was built using AutoCAD software, and then files were exported in SAT format and input into ANSYS/LS-DYNA. Finally, attributes and element types were defined into SHELL 163 element, and material type was input into the bilinear servo strengthening material model. Finally, the mesh was divided.

Then, a numerical model was developed based on the S-J method for roof sheathing where the key point positions of roof sheathing were determined according to the key point positions of members. Half of the node height (0.25 m) was added along the Z-axis direction, and roof sheathing was 0.002 m thick. Then, triangular roof sheathing was formed based on key points according to the geometry of roof sheathing. Roof sheathing and nodes were welded. The connections between each members of whole structure were accomplished using NUMMRG command.

During the collision, the reticulated dome was divided into impact and nonimpact zones such that the area covering the members and joints where the airplane collided was considered as the impact zone and the remaining area was the nonimpact zone [19]. The failure mode in the reticulated dome during collision included local denting, punching failure, and collapse [11].

Because of the low height of reticulated domes, aircraft have to decelerate to impact. Different impact velocities of 80, 100, and 120 m/s were tested. The flight patterns of passenger planes are usually horizontal, and if the impact takes place in this mode, we call it impact mode 1. However, due to uncertainties of flight situations, the subduction posture of the passenger plane was considered, and if the

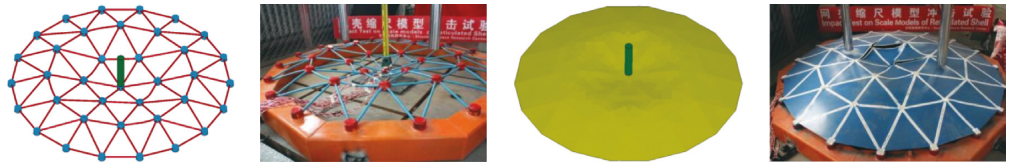

(a) (b) (c) (d)

Figure 6: Comparison of the failure model of the reticulated dome. Without roof sheathing: (a) numerical results and (b) test results. With roof sheathing: (c) numerical results and (d) test results.

Table 4: Impact mode and velocity of aircraft.

Number	Angle of tilt	Flight attitude and impact mode	Velocity (m/s)
Impact mode 1	30°	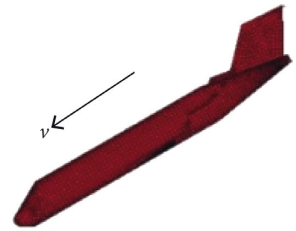	80 100 120
Impact mode 2	0°		80 100 120

impact takes place in this mode, we call it impact mode 2, as shown in Table 4. The third ring of the reticulated dome was the most vulnerable position, and the nodes on this ring were simulated using impact modes 1 and 2.

The impact zone of aircraft and spherical joints are shown in Figure 7. N4 was chosen as the impact point, and the nodes located along the impact direction were N1, N2, N3, N4, N5, N6, and N7. The nodes symmetrical to the impact direction (except N1) were N2′, N3′, N4′, N5′, N6′, and N7′.

4.2. Failure Modes under Different Impact Types. The failure processes of the main member of a reticulated dome under oblique impact at different velocities are shown in Figure 8. The member bar was broken by the aircraft head, and aircraft subsequently crashed into the reticulated dome. All members around the impact zone were sunk.

At the speed of 120 m/s, after node N4 was impacted by the aircraft head, the members of rings 3 and 4 were impacted by the airfoil; then, the members of rings 1 and 2 were impacted by empennage expanding damage area. Rings 1 to 4 in the impact zone exhibited a large depression area and most of the members failed. Rings 5 and 6 had no depression, but some of their members were also deformed. Since the reticulated dome had a large depression area, the members located in the impact zone failed and the impact zone was penetrated, resulting in the integer collapse of the reticulated dome.

Damage processes in reticulated domes under horizontal impacts at different velocities are shown in Figure 9. After the aircraft head rushed into the reticulated dome at the

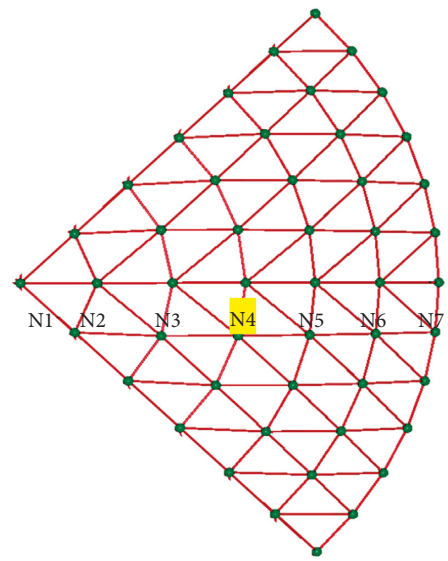

Figure 7: Serial number of nodes in the reticulated shell.

velocity of 80 m/s, roof sheathing and members exhibited large deformations when punched with the airfoil. Adjacent members were less affected, and the whole roof sheathing was wrinkled and displaced along the impact direction. Aircraft was encased by roof sheathing, and members in the impact zone were damaged, while members of other zones exhibited insignificant deformations. At the collision velocity of 100 m/s, nodes N4, N3, N2, N1, N2′, N3′, N4′, and N5′ were impacted by the aircraft head. Members around

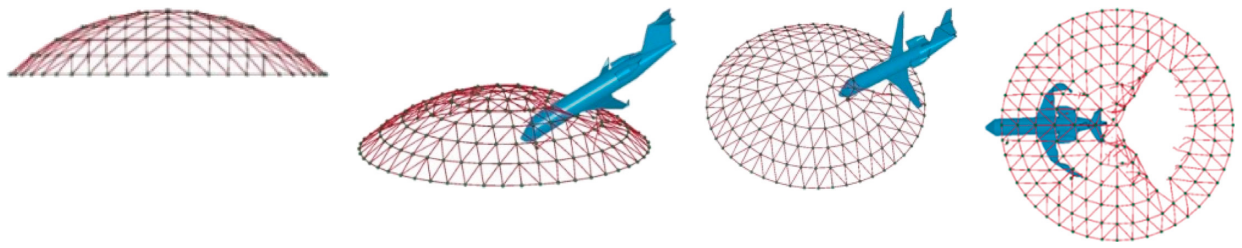

(a) (b) (c) (d)

Figure 8: Deformations in the reticulated dome under oblique impact at different velocities. Main bars (a) before impact, (b) after 80 m/s impact, (c) after 100 m/s impact, and (d) after 120 m/s impact.

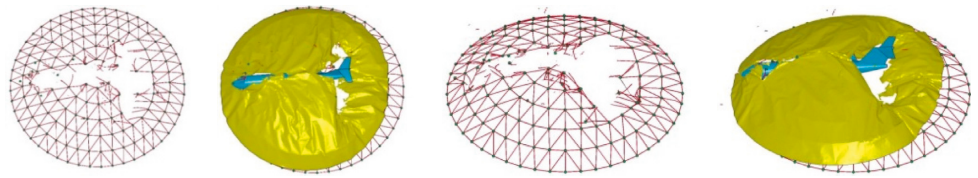

(a) (b) (c) (d)

Figure 9: Deformations in the reticulated dome under lateral impact at different velocities. (a) Main bars after 80 m/s impact. (b) Structure after 80 m/s impact. (c) Main bars after 120 m/s impact. (d) Structure after 120 m/s impact.

these nodes were snapped; then, nodes and members on rings 2 and 3 were cut by the airfoil, and finally, members on ring 1 were impacted by the empennage. The reticulated dome was penetrated, and most of the structural components on rings 1 to 3 were failed. The destruction of the reticulated dome from the impact zone to the support all lead to deformation, resulting in collapse.

Nodes N4 to N5′ were continuously impacted by the aircraft head during horizontal impact at 120 m/s. The top of the reticulated dome was divided into two parts, the members of rings 4-5 were cut by the airfoil and exhibited large deformations, and those on rings 1-2 were impacted by the empennage. Finally, the velocity of the aircraft was greatly reduced after its head rushed out of the reticulated dome, and the aircraft was "trapped" in the structure. The reticulated dome was penetrated, and most members and roof sheathings were damaged resulting in its collapse.

5. Dynamic Response Analysis during Impact

5.1. Velocity-Time History Analysis of Spherical Joints. The displacement curve of ball nodes along two impact directions at the impact velocity of 80 m/s is shown in Figure 10. The stress wave was spread from the impact zone to the other parts of the reticulated dome under oblique impact, and its magnitude was gradually decreased by distance. At N4, peak velocity was instantaneously reached because it was located at the impact zone. Peak velocity was then spread from N4 to other nodes, and its velocity values were gradually decreased with the increase of distance. Nodes N1, N2, N6, and N7 did not show significant movements. The aircraft head was collided with N3 at 0.08 s, and peak velocity was reached at 0.11 s.

The spread of the stress wave at symmetric nodes was gradually decelerated. Under different conditions, symmetric nodes were nearly stationary, but their peak velocities were reached almost simultaneously.

Under horizontal impact also, the stress wave was spread from the impact zone to other parts of the reticulated dome, but its magnitude was gradually decreased. The aircraft head collided with N3 at 80 m/s after 0.06 s causing a dramatic change in its velocity. Velocity at N5 was changed gently and reached 10 m/s. Due to the low initial velocity of the aircraft, no obvious disturbance was witnessed in nodes N1, N2, N6, and N7. At the impact velocities of 100 and 120 m/s, the peak velocity of N4 was reached instantaneously. Peak velocities were then reached at nodes N3, N2, and N1, respectively. The velocities of N5 and N6 were changed gently. N7 remained almost stationary.

The stress wave at symmetric nodes was spread from the impact zone to other parts of the reticulated dome, and its magnitude was decreased with distance. At the impact velocity of 80 m/s, symmetric nodes reached their peak velocities almost simultaneously, but their overall magnitudes were gradually decreased. At the impact velocities of 100 and 120 m/s, symmetric nodes remained almost stationary before node N1 was impacted. However, after N1 node was impacted, other nodes reached their peak velocities with their overall magnitudes decreasing gradually. Nodes N6′ and N7′ were almost stationary.

When the structure was obliquely impacted by aircraft at different velocities, the peak velocities of spherical joints along the impact direction were reached according to their distance from the impact zone. The velocities of nodes near the impact point were changed dramatically, and those far from it experienced minor velocity changes. The aircraft head collided with N3 at 80 m/s after 0.08 s, and peak velocity was reached after 0.11 s. The peak velocity of the corresponding symmetric node was reached almost simultaneously, and the dynamic responses of nodes near the

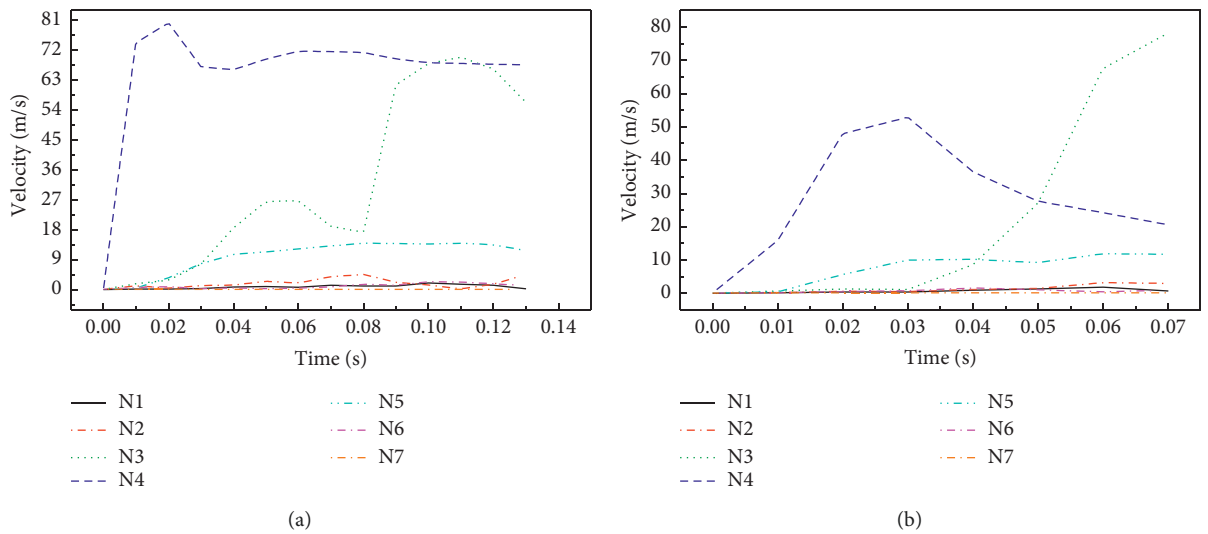

Figure 10: Velocity of ball nodes along the impact direction at 80 m/s. (a) Oblique impact. (b) Lateral impact.

support were relatively lower. When the structure was horizontally impacted, the aircraft head collided with N1, N2, N3, and N4 and the spherical joints received high kinetic energies resulting in velocity increase. The velocities of other nodes were changed gently, and each node reached its peak velocity based on its distance from the impact zone with its overall magnitude decreasing with distance. Higher initial aircraft velocities resulted in greater velocity changes in the structure. In conclusion, the stress wave was spread from the impact zone to supports and its magnitude was decreased with distance.

5.2. Displacement Analysis of Spherical Joints. The displacements of spherical joints in the two investigated impact modes at 80 m/s are shown in Figure 11. The stress wave under oblique impact was spread from the impact zone to the other parts of the reticulated dome, and its magnitude was decreased gently with distance. Under different conditions, the displacement of impact site (N4) was proportional to time, which drove the surrounding spherical joints. Displacement values reached their peaks synchronously and were decreased with distance from the impact zone; i.e., the displacements of N1, N2, N6, and N7 were gently changed. N3 was contacted with the aircraft head at 80 m/s after 0.08 s causing the velocity of symmetric node N3 to be greater than that of N5.

The stress wave of symmetric nodes was gradually decreased as the wave continued to spread. The displacements of symmetric nodes were lower under different conditions, but peak displacements were reached almost simultaneously. In conclusion, the displacements of the nodes were decreased with their distance from the impact zone.

The displacement of N4 at the impact zone during horizontal impact at 80 m/s was changed obviously which drove the surrounding spherical joints. Because N3 was impacted at 0.06 s, its displacement was obviously higher than that of N5 which was impacted later. Due to the lower initial velocity of the aircraft, the responses of nodes N1, N2, N6, and N7 were not significant. N4 was first displaced after impacts at 100 and 120 m/s, but nodes N1, N2, and N3 were detached from the reticulated dome due to collision with the aircraft head, and their displacement values were continuously increased and finally exceeded that of N4. The displacements of N5 and N6 were changed gently and reached their peak values based on their distance from the impact zone. No obvious displacement was observed at node N7, which was near the support.

The magnitude of the stress wave in symmetric nodes was decreased gradually as the wave was spread. Under different conditions, the displacements of N2′, N3′, N4′, and N5′ were changed dramatically after N1 was impacted and their peak displacements were reached almost simultaneously with their values being decreased with their distance from the impact zone. N6′ and N7′ remained almost stationary.

When the aircraft collided obliquely with the structure, only N4 was impacted by the aircraft head. Nodes along the impact direction were driven by the impact zone and synchronously reached their peak displacement values. Symmetric nodes remained almost stationary because they did not contact with the aircraft. However, when the aircraft collided horizontally with the structure, nodes N4 to N1 were impacted continuously by the aircraft head, and their peak displacements were reached based on their impact order. The displacements of spherical joints along the symmetric direction were changed dramatically after collision with N1 and reached their peak values based on their impact order. The responses of spherical joints were greater for higher initial velocities of aircraft. Larger distances between farther spherical joints and the impact zone resulted in smaller impact responses. In conclusion, the stress wave was spread from the impact zone to support, and its magnitude was decreased with distance.

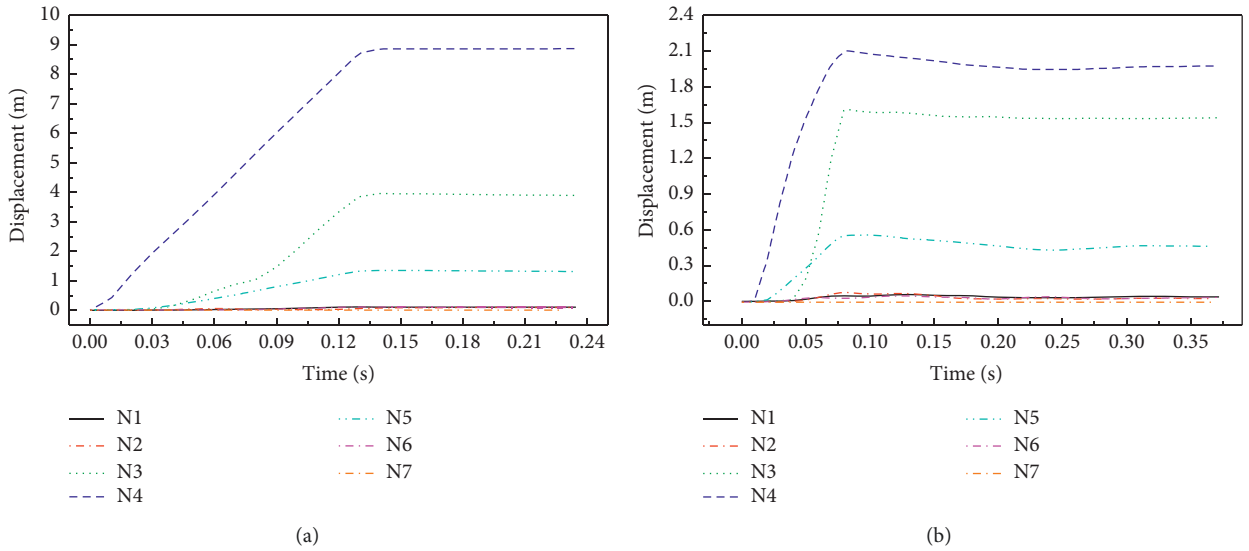

Figure 11: Displacement of ball nodes along the impact direction at 80 m/s. (a) Oblique impact. (b) Lateral impact.

Table 5: Energies of the ball nodes, bars, and roof panel under oblique impact with different velocities.

Velocity (m/s)	Time (s)	Spherical joints (MJ)	Members (MJ)	Roof sheathing (MJ)	Ratio
80	0.02	0.698	0.562	0.479	1.24 : 1 : 0.85
	0.05	0.648	0.62	0.856	1.04 : 1 : 1.38
	0.09	1.423	1.044	1.338	1.36 : 1 : 1.28
	0.13	1.100	1.133	1.305	0.97 : 1 : 1.15
100	0.01	0.999	0.31	0.430	3.27 : 1 : 1.42
	0.05	0.989	0.754	1.200	1.31 : 1 : 1.59
	0.10	1.020	0.945	1.200	1.08 : 1 : 1.27
120	0.05	1.610	0.679	1.174	2.364 : 1 : 1.7
	0.11	3.722	1.297	3.190	2.87 : 1 : 2.46
	0.20	4.785	3.442	8.030	1.39 : 1 : 2.33
	0.29	5.150	4.597	9.639	1.12 : 1 : 2.1
	0.36	4.880	4.923	10.02	0.991 : 1 : 2

5.3. Energy Variation of Reticulated Dome. The reticulated dome was horizontally and obliquely impacted by aircraft at the velocities of 80, 100, and 120 m/s, and the kinetic and deformation energies [20] of its members, spherical joints, and roof sheathing were analyzed. The energies of different parts of the structure under oblique impact at different times are summarized in Table 5.

At 80 m/s, the area of the roof sheathing impacted by the aircraft head was small at 0.02 s, and the energy acquired by the roof sheathing was less than that received by members. As the contact area between aircraft and roof sheathing was increased, the energy acquired by it was increased and reached the maximum value among the three structural components. Nodes N4, N3, N2, and N1 were, respectively, impacted by the aircraft head, and spherical joints received high kinetic energies, but its value was decreased gradually until it reached the energy of members. At 100 m/s impact velocity, the aircraft first contacted the spherical joints and nodes received maximum energy. Then the aircraft rushed into the reticulated dome, and the impact area of roof sheathing was expanded increasing its energy to a maximum value. Table 5 shows that the energy ratio of the spherical joint and member was 2.346 : 1 at 0.05 s because spherical joints were first impacted by the aircraft head at 120 m/s. Members constantly received energy as the aircraft pushed along its path, and the final energy ratio of the spherical joint and member became 0.991 : 1. The energy of roof sheathing was always twice as much as that of members, and the energy variation of roof sheathing reached the maximum value among the three structural compartments.

The energy variations of reticulated dome members, spherical joints, and roof sheathing for different impact velocities at different times are summarized in Table 6. The contact area of roof sheathing under horizontal impact at 80 m/s was larger, and its energy was maximum among the three structural compartments. Because N4 was located at the impact zone and was first contacted with the aircraft head, its initial energy was higher than surrounding members. At 100 m/s impact, the aircraft head rushed into the reticulated dome at 0.05 s and mainly contacted with spherical joints. The energy ratio of members and roof

Table 6: Energy and contrast of ball nodes, bars, and roof panel under aircraft impact at different velocities.

Velocity (m/s)	Time (s)	Spherical joints (MJ)	Members (MJ)	Roof sheathing (MJ)	Ratio
80	0.02	0.238	0.121	0.235	1.97 : 1 : 1.94
	0.05	0.298	0.449	0.686	0.66 : 1 : 1.53
100	0.05	1.436	0.848	0.852	1.69 : 1 : 1
	0.11	1.773	1.316	2.081	1.35 : 1 : 1.58
	0.18	5.21	3.397	6.65	1.53 : 1 : 1.96
	0.27	10.41	5.724	9.205	1.82 : 1 : 1.61
	0.36	8.505	6.823	12.24	1.25 : 1 : 1.87
120	0.01	0.210	0.075	0.210	2.8 : 1 : 1
	0.10	3.780	1.670	2.410	2.26 : 1 : 1.44
	0.18	9.710	4.540	7.300	2.14 : 1 : 1.61
	0.23	12.24	5.830	10.09	2.15 : 1 : 1.73
	0.29	6.470	5.120	8.050	1.26 : 1 : 1.57

sheathing was 1 : 1 under this condition. With the continuous impact of aircraft, the impact area of roof sheathing was increased and its energy variation was the largest among the three structural compartments. At 120 m/s, spherical joints N4, N3, N2, N1, N2′, N3′, and N4′ were impacted continuously by the aircraft head and their kinetic energies became higher than that of surrounding members and roof sheathing. The energies of spherical joints were about double that of members before the collision was ended, and the final energy ratio of spherical joints to members became 1.26 : 1. Because the contact area between reticulated dome and aircraft head was small at 0.01 s, the energy ratio of members and roof sheathing was 1 : 1. The energy of roof sheathing was about 1.5 times higher than that of members during continuous impact. The energy variations of spherical joints were the largest among the three structural compartments during impact, and roof sheathing had the highest energy after collision was ended.

In most of the conditions, the energies of spherical joints and roof sheathing were higher than those of members. Hence, spherical joints and roof sheathing had to be considered during research on the dynamic responses of reticulated domes during aircraft collisions.

6. Conclusions

In this paper, the dynamic responses of single-layer reticulated domes to aircraft collisions under different conditions were systemically investigated. The main conclusions drawn in this work can be summarized as follows:

(1) The S-J method was proposed for reticulated domes under aircraft impacts with the Johnson–Cook model for material properties and SHELL 163 element as the members of a numerical model for these structures; shell elements were used as spherical joints in reticulated shells.

(2) A numerical reticulated dome scale model with and without roof sheathing under elastic and destructive impacts was developed based on the S-J method. During elastic impact, the impact duration, stress peaks, and impact time intervals obtained from the two reticulated dome models were compared with results obtained from the drop-weight test, and it was observed that the errors of the proposed method were lower than those of the B-P method. During destructive impact, the failure mode was similar to test results, i.e., the reticulated dome without roof sheathing was collapsed and that with roof sheathing was locally dented. Hence, the validity of the S-J modeling method was verified.

(3) A numerical model which was developed for a Bombardier Challenger 850 small aircraft was used to examine its collision with a reticulated dome constructed with the S-J method. The failure mode and dynamic response of the reticulated dome under horizontal and oblique impacts of the aircraft at different velocities were also investigated. The displacements and velocities of spherical joints and the stresses of members in the impact zone were very high, which easily caused the collapse of the reticulated dome after impact. Various ratios of members, spherical joints, and roof sheathing were examined. In most conditions, the energies of spherical joints and roof sheathing were higher than those of members.

(4) The results obtained in this study showed that the effects of temperature, spherical joints, and roof panels on the dynamic responses of reticulated dome had to be considered during studying aircraft collisions.

Data Availability

The data used to support the findings of this study are included within the article.

Conflicts of Interest

The authors declare that they have no conflicts of interest.

Acknowledgments

The authors wish to acknowledge the support from the National Science Foundation of Heilongjiang Province of China (nos. LH2019E060 and 201438) and the National

Natural Science Foundation of China (Grant nos. 11502120 and 51578515).

References

[1] S. Z. Shen and X. Chen, *Structural Stability of Reticulated Shells*, Science Press, Beijing, China, 1999.

[2] Y. G. Zhang, D. S. Xue, and Q. S. Yang, *Large-Span Spatial Structure*, Mechanical Industry Press, Beijing, China, 2005.

[3] X. M. Zhai and Y. H. Wang, "Modelling and dynamic response of steel reticulated shell under blast loading," *Shock and Vibration*, vol. 20, no. 1, pp. 19–28, 2013.

[4] X. M. Zhai and M. Huang, "Protective measures for reticulated shell subjected to internal blast loading," *Journal of Harbin Institute of Technology*, vol. 45, no. 2, 2013.

[5] G. B. Nie and K. Liu, "Experimental studies of single-layer reticulated domes with isolated supports," *Shock and Vibration*, vol. 2018, Article ID 6041878, 15 pages, 2018.

[6] L. L. Xu and J. H. Ye, "DEM algorithm for progressive collapse simulation of single-layer reticulated domes under multi-support excitation," *Journal of Earthquake Engineering*, vol. 23, no. 1, pp. 18–45, 2017.

[7] L. Le, X. Gao, and W. Wang, "Study on explosion effects of a spherical reticulated shell under internal explosions," *International Journal of Civil Engineering*, vol. 16, no. 12, pp. 1713–1724, 2018.

[8] H. W. Li, K. Guo, J. W. Wei, and D. Q. Qin, "The dynamic response of a single-layer reticulated shell to drop hammer impact," *Explosion and Shock Waves*, vol. 26, no. 1, pp. 39–45, 2006.

[9] K. Guo, *Dynamic Response Analysis of Single-Layer Reticulated Shells under Impact*, Taiyuan University of Technology, Taiyuan, China, 2004.

[10] W. Li, X. Zhi, D. Wang, F. Fan, and S. Shen, "Static stability analysis of a reticulated shell with a roofing system," *Engineering Structures*, vol. 185, pp. 315–331, 2019.

[11] D. Z. Wang, *Failure Mechanism of Reticulated Dome under Impact*, Harbin Institute of Technology, Harbin, China, 2010.

[12] X. L. Wang, F. Q. Zhang, and W. W. Yang, "Dynamic response analysis of single-layer spherical reticulated shell with sub steel column under impact load," *Journal of Architecture and Civil Engineering*, vol. 32, no. 3, pp. 21–26, 2015.

[13] C. Wu, X. L. Wang, X. T. Ma, and Y. X. Liang, "Numerical analysis and experimental study on the dynamic response of single-layer reticulated shell under impact," *Journal of Vibration and Shock*, vol. 33, no. 22, pp. 88–96, 2014.

[14] L. Lin, *Refined Study on Impact Response and Failure of Reticulated Shells*, Harbin Institute of Technology, Harbin, China, 2015.

[15] L. Lin, F. Fan, X. Dong Zhi, and H. Feng Yin, "Size effect and material property effect of the impactor on the damage modes of the single-layer kiewitt-8 reticulated dome," *Research Journal of Applied Sciences, Engineering and Technology*, vol. 7, no. 3, pp. 515–520, 2014.

[16] H. F. Yin, *Loading Model of Dynamic Response of Single-Layer Reticulated Domes under Impact Loads*, Harbin Institute of Technology, Harbin, China, 2012.

[17] L. Lin, X. D. Zhi, F. Fan, S. J. Meng, and J. J. Su, "Determination of parameter of Johnson-Cook models of Q235B steel," *Journal of Vibration and Shock*, vol. 33, no. 9, pp. 153–159, 2014.

[18] S. Q. Shi, J. G. Kang, and M. Wang, *Engineering Application of Ansys/ls-dyna in the Field of Explosion and Shock*, vol. 49, China Architecture and Building Press, Beijing, China.

[19] Y. H. Sun, *Dynamic Analysis of Kiewitt Single-Layer Reticulated Dome under Aircraft Impact*, Harbin University of Science and Technology, Harbin, China, 2017.

[20] D. Z. Wang, X. D. Zhi, F. Fan, and S. Z. Shen, "Failure process and energy transmission for single-layer reticulated domes under impact loads," *Transactions of Tianjin University*, vol. 14, no. S1, pp. 551–557, 2008.